



The florigen interactor BdES43 represses flowering in the model temperate grass *Brachypodium distachyon*

Shuanghe Cao^{1,*†} , Xumei Luo^{1,†}, Li Xie^{1,†}, Caixia Gao², Daowen Wang², Ben F. Holt III³, Hao Lin⁴, Chengcai Chu²  and Xianchun Xia¹

¹National Wheat Improvement Center, Institute of Crop Sciences, Chinese Academy of Agricultural Sciences (CAAS), 12 Zhongguancun South Street, Beijing 100081, China,

²Institute of Genetics and Developmental Biology, Chinese Academy of Sciences (CAS), No. 1 West Beichen Road, Chaoyang District, Beijing 100101, China,

³Department of Microbiology and Plant Biology, University of Oklahoma, 770 Van Vleet Oval, Norman, OK 73019, USA, and

⁴Biotechnology Research Institute, Chinese Academy of Agricultural Sciences (CAAS), 12 Zhongguancun South Street, Haidian District, Beijing 100081, China

Received 19 December 2018; revised 25 October 2019; accepted 5 November 2019; published online 29 November 2019.

*For correspondence (e-mail caoshuanghe@caas.cn).

†These authors contributed equally to this work.

SUMMARY

FLOWERING LOCUS T (FT) protein, physiologically florigen, has been identified as a system integrator of numerous flowering time pathways in many studies, and its homologs are found throughout the plant lineage. It is important to uncover how precisely florigenic homologs contribute to flowering initiation and how these factors interact genetically. Here we dissected the function of *Brachypodium* FT orthologs *BdFTL1* and *BdFTL2* using overexpression and gene-editing experiments. Transgenic assays showed that both *BdFTL1* and *BdFTL2* could promote flowering, whereas *BdFTL2* was essential for flowering initiation. Notably, *BdFTL1* is subject to alternative splicing (AS), and its transcriptional level and AS are significantly affected by *BdFTL2*. Additionally, *BdFTL2* could bind with the PHD-containing protein BdES43, an H3K4me3 reader. Furthermore, *BdES43* was antagonistic to *BdFTL2* in flowering initiation in a transcription-dependent manner and significantly affected *BdFTL1* expression. *BdFTL2*, *BdES43* and H3K4me3 also had highly similar distribution patterns within the *BdFTL1* locus, indicating their interplay in regulating target genes. Taken together, florigen *BdFTL2* functions as a potential epigenetic effector of *BdFTL1* by interacting with a *BdES43*-H3K4me3 complex. This finding provides an additional insight for the regulatory mechanism underlying the multifaceted roles of florigen.

Keywords: *Brachypodium*, *BdES43*, H3K4me3, florigen, flowering time, gene editing.

INTRODUCTION

Flowering is crucial for the reproductive success of plants, and the proper timing of flowering determines environmental adaptation and agronomic productivity in crop plants. Genetic regulation of flowering mainly includes five pathways: photoperiod, vernalization, gibberellin, autonomy and age (Fornara *et al.*, 2010; Pin and Nilsson, 2012). FT protein, physiologically florigen, functions as a hub to determine flowering initiation in all plants where flowering time genes have been investigated (Fornara *et al.*, 2010; Srikanth and Schmid, 2011; Wigge, 2011; Andres and Coupland, 2012; Pin and Nilsson, 2012; Song *et al.*, 2015).

Brachypodium distachyon (hereafter *Brachypodium*) is a wild grass species and a model of temperate crops, such

as wheat and barley (IBI, 2010; Brkljacic *et al.*, 2011; IWGSC, 2014). Comparative genomic analyses identified 18 FT homologs in the *Brachypodium* accession Bd21, and *BdFTL1* (Bradi2g07070) and *BdFTL2* (Bradi1g48830) had the highest similarity with previously reported flower-promoting FT genes (Higgins *et al.*, 2010). Transcriptional analyses showed a high association of *BdFTL2* with the flowering time of distinct accessions from different areas (Schwartz *et al.*, 2010). Recently, *BdFTL2* was identified as a candidate gene underlying a major QTL for flowering time (Bettgenhaeuser *et al.*, 2017). Additionally, overexpression (OE) of *BdFTL2* promoted flowering (Ream *et al.*, 2014), and RNAi experiments confirmed that *BdFTL2* was critical in controlling flowering time (Lv *et al.*, 2014). Furthermore, both

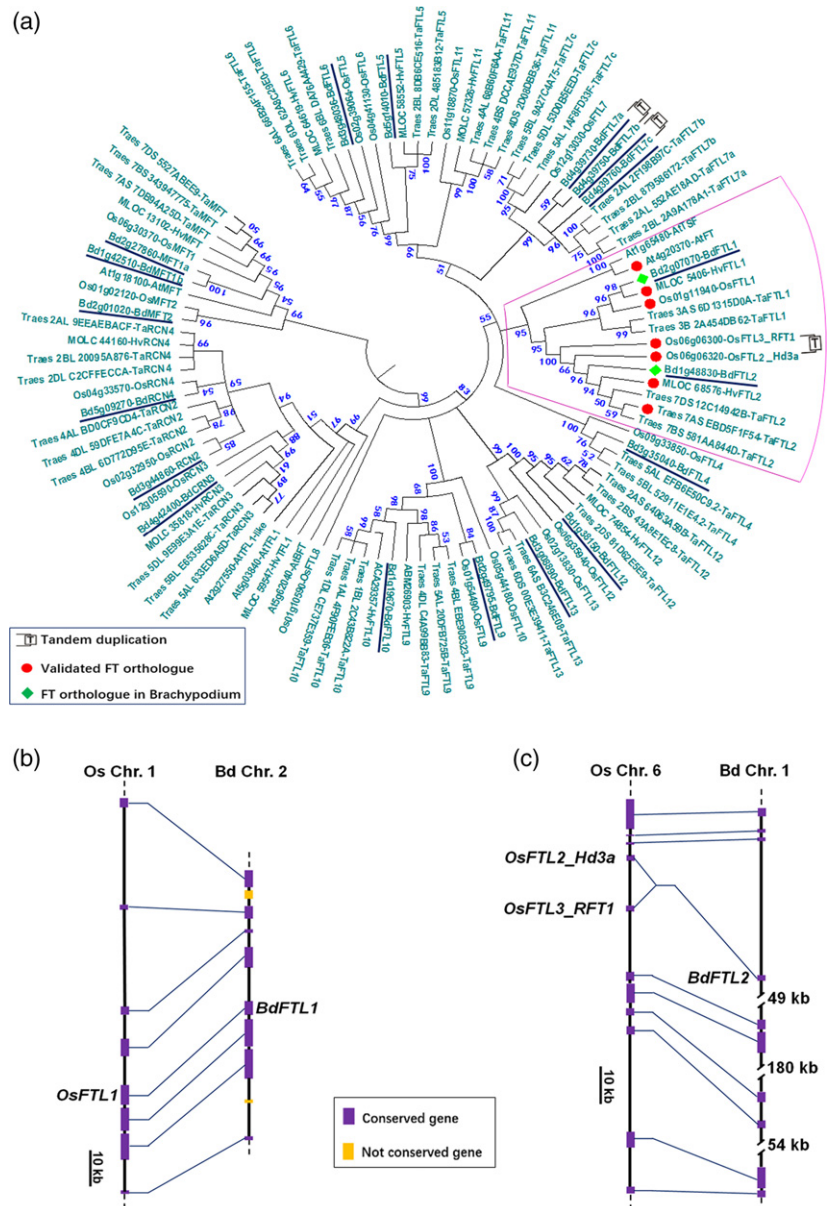
BdFTL1 and *BdFTL2* were targeted by miR5200 and could promote flowering, indicating redundant function of the two *FT*-like genes in flowering (Wu *et al.*, 2013). OE of *BdFTL2* could also rescue the non-flowering *phyC* mutant phenotype, consistent with it being an important downstream photoperiod integrator (Woods *et al.*, 2014). Further, *BdFTL1* was undetectable in the *phyC* background; thus, loss of *BdFTL1* expression might also contribute to the delayed flowering phenotype of the *phyC* mutant (Woods *et al.*, 2014). However, it is still unclear how precisely florigenic homologs contribute to flowering initiation and how these factors interact genetically. Here our objective was to better understand the individual effects of *BdFTL1* and *BdFTL2* on flowering, their genetic relationship and regulatory machinery.

Figure 1. Phylogenetic and synteny analyses of *FT* homologs.

(a) Neighbor-joining tree of *FT* and related proteins in *Brachypodium distachyon* (Bd), *Triticum aestivum* (Ta), *Hordeum vulgare* (Hv), *Oryza sativa* (Os), *Setaria italica* (Si), *Sorghum bicolor* (Sb), *Zea mays* (Zm) and *Arabidopsis thaliana* (At). The phylogenetic tree was constructed based on the multiple alignments of protein conserved regions using the software Clusl W following Higgins *et al.* (2010). The purple box shows the sub-branch including functionally validated *FT* proteins. All *Brachypodium* *FT* homologs are underlined.

(b) Collinearity analysis of *FT* gene-containing region in rice chromosome 1 with the orthologous regions of *Brachypodium* chromosome 2.

(c) Collinearity analysis of *FT* gene-containing region in rice chromosome 6 with the orthologous regions of *Brachypodium* chromosome 1. Note: here the names of *Brachypodium* *FT* homologs follow the rice nomenclature system.



RESULTS

BdFTL1 and *BdFTL2* have the highest homology with known florigens

To examine the homologs of *FT* genes in *Brachypodium*, we performed a phylogenetic analysis across major crops in the temperate grass family as well as the model plants *Arabidopsis* and rice. In the phylogenetic tree, most function-validated *FT* homologs are grouped in the same monophyletic clade and there are two members for each species, except that rice possessed three due to a tandem duplication event (Figure 1a; Dataset S1). Among them, *BdFTL1* and *BdFTL2* are the two *FT* homologs with the highest similarity to known florigens, such as *AtFT* and *Hd3a* (Corbesier *et al.*, 2007; Tamaki *et al.*, 2007). Genomic

synteny analyses also validated that *BdFTL1* and *BdFTL2* were orthologous with rice florigen genes (Figure 1b,c; Dataset S2).

Both *BdFTL1* and *BdFTL2* enable flowering initiation

In previous studies, OE experiments demonstrated that both *BdFTL1* (Wu *et al.*, 2013) and *BdFTL2* (Wu *et al.*, 2013; Lv *et al.*, 2014; Ream *et al.*, 2014) sufficed to promote flowering. We observed the same result in initial experiments using the ZmUbi promoter (Figure 2a); however, as

previously reported, no seeds were obtained because the T_0 lines flowered too early to presumably generate the biomass needed for seed production (Wu *et al.*, 2013; Lv *et al.*, 2014). Because the 35S promoter drives considerably lower expression than ZmUbi in grasses (Christensen *et al.*, 1992; Alves *et al.*, 2009), we developed 35S promoter-driven *BdFTL1* and *BdFTL2* constructs. Ten OE lines each for *BdFTL1* and *BdFTL2* were used to investigate phenotypic data. As with the ZmUbi-driven constructs, both *p35S:BdFTL1* and *p35S:BdFTL2* significantly promoted early

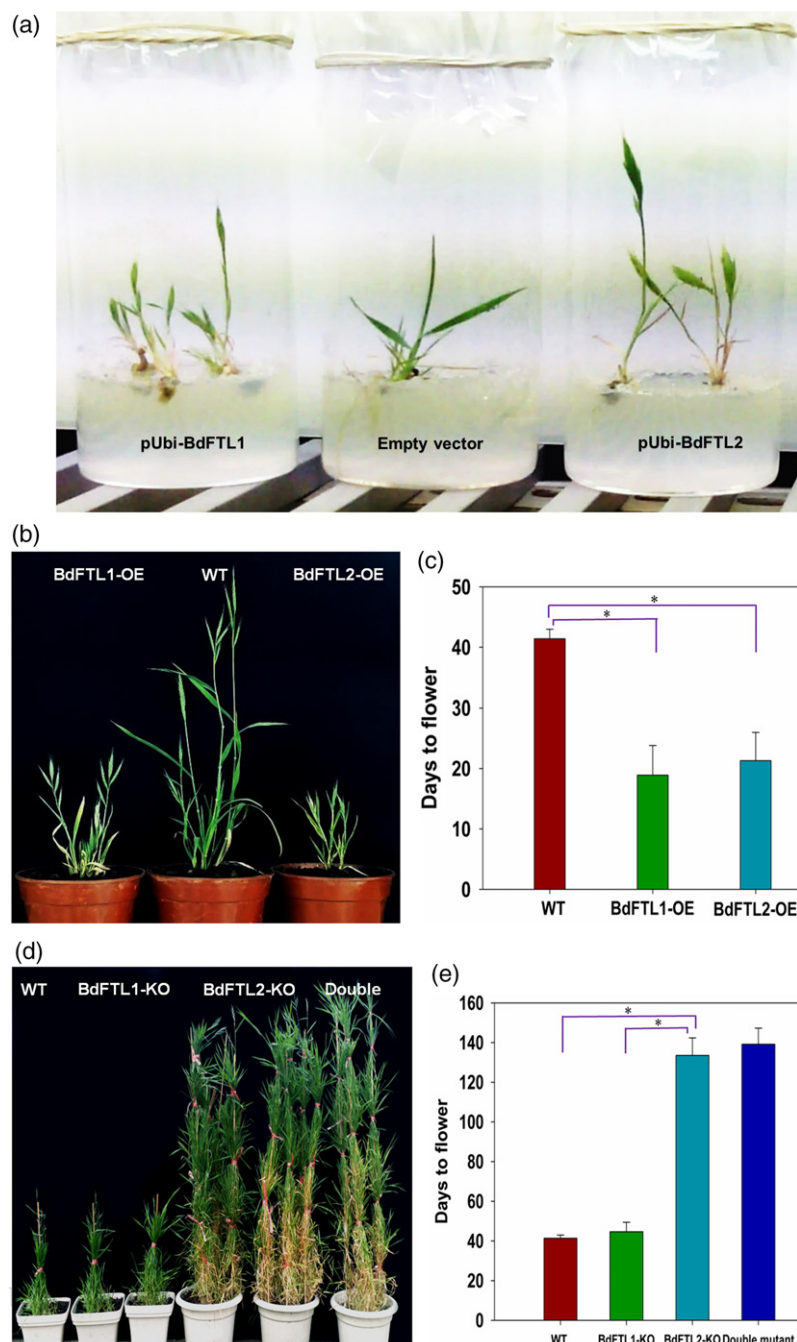


Figure 2. Phenotypes of *BdFTL1* and *BdFTL2* over-expression (OE) and knockout (KO) lines.

(a) Phenotypes of transgenic lines of *BdFTL1* and *BdFTL2* driven by the ZmUbi promoter. pUbi-BdFTL1 and pUbi-BdFTL2 represent the constructs of ZmUbi promoter-driven *BdFTL1* and *BdFTL2*, respectively.

(b) Representative plants from transgenic lines of *BdFTL1* and *BdFTL2* driven by the 35S promoter. The representative plants for wild-type (WT), *BdFTL1* OE and *BdFTL2* OE lines are approximately 45, 25 and 25 days old, respectively, post-seed germination.

(c) Days to flowering of WT, *BdFTL1*-OE and *BdFTL2*-OE lines.

(d) Representative plants for *BdFTL1* knockout (KO) and *BdFTL2*-KO lines. The two independent lines for each of *BdFTL1* KO and *BdFTL2* KO were used to display their phenotypes. The representative plants for WT, *BdFTL1* KO, *BdFTL2* KO and double KO are approximately 45, 45, 140 and 140 days old, respectively.

(e) Days to flowering of WT, *BdFTL1*-KO and *BdFTL2*-KO lines. *Labeled significant difference at $P = 0.05$. The double-mutants of *BdFTL1* and *BdFTL2* were generated from the hybridization between their respective mutant lines. *BdFTL1* KO lines had comparable flowering times to WT lines ($P = 0.054$ in Dataset S3). Flowering times of *BdFTL2* KO lines were not significantly different from those of the double-mutants ($P = 0.054$ in Dataset S3). The transcriptional level of *BdFTL1* showed the total of normal and alternative splicing (AS) transcripts using quantitative polymerase chain reaction (qPCR) with a primer pair targeting the overlapping region of the two transcripts (Figure S3; Table S4).

flowering (Figure 2b,c; Dataset S3). Additionally, we successfully obtained transgenic seeds, facilitating the following investigations.

***BdFTL2* plays a pivotal role in flowering initiation**

To further reveal the respective effects of *BdFTL1* and *BdFTL2* on flowering, we created gene-specific knockout (KO) lines using TALEN technology (Figure S1). Ten KO (truncation and/or frameshifts) homozygous lines each for *BdFTL1* and *BdFTL2* were used to investigate flowering time. Strikingly, *BdFTL2*-KO lines did not flower for approximately 3 months under inductive long-day (LD) conditions, whereas *BdFTL1*-KO lines had comparable flowering times to the wild-type (WT; $P = 0.0540$ in Dataset S3; Figure 2d,e), although *BdFTL1* KO delayed flowering by more than 5 days compared with WT (Dataset S3). We additionally examined the flowering time phenotypes of eight *BdFTL1* and *BdFTL2* double-mutants. The flowering times of the double-mutant lines were similar to that of *BdFTL2*-KO lines ($P = 0.0540$ in Dataset S3; Figure 2d,e). Moreover, we compared the flowering time of *BdFTL1*-KO, *BdFTL2*-KO and WT lines under short-day conditions, and observed that *BdFTL2*-KO lines also flower later than WT lines, while *BdFTL1*-KO lines have similar flowering time to WT lines (Figure S2). Thus, *BdFTL1* appears to be dispensable for flowering, but *BdFTL2* is critical to initiate flowering.

***BdFTL1* and *BdFTL2* display similar transcriptional patterns**

To explore the underlying reason for the differences between *BdFTL1* and *BdFTL2* in flowering initiation, we investigated their transcription patterns under inductive LD conditions. From previous research, we expected florigenic *FT* expression in leaves, with a significant daily response to photoperiod and a gradual increase prior to flowering (Corbesier *et al.*, 2007; Tamaki *et al.*, 2007). Initially we tested the transcriptional activities of *BdFTL1* and *BdFTL2* in different tissues and observed similar tissue-specific expression profiles: mainly expressing in leaves, relatively low transcriptional activity in stems, and rarely expressing in roots (Figure 3a; paired *t*-test $P = 0.0578$ in Table S1). We further investigated the time-course transcriptional variation of *BdFTL1* and *BdFTL2* over a full day under LD conditions. Both genes had significant responses to the light/dark shift with similar transcriptional patterns, including an incremental increase in mRNA accumulation, peaking at end of day, and then a gradual decline in the dark (Figure 3b; paired *t*-test $P = 0.1489$ in Table S1). The transcriptional levels of *BdFTL1* and *BdFTL2* in different developmental phases were also measured. Quantitative polymerase chain reaction (qPCR) indicated that *BdFTL2* transcription activity was comparatively stronger than *BdFTL1* in the

corresponding period; however, their transcription activities in different developmental phases were similar, i.e. increasing over developmental time before flowering (Figure 3c; paired *t*-test $P = 0.7186$ in Table S1). Overall, *BdFTL1* and *BdFTL2* had similar transcription patterns in different tissues, developmental phases, and during responses to the light/dark shift, indicating that transcriptional regulation was not likely to be the key element causing large functional differences in flowering.

***BdFTL1* is subject to mRNA alternative splicing**

Because transcriptional regulation was not the obvious determinant for the functional discrepancy between *BdFTL1* and *BdFTL2*, we compared their post-transcriptional activities. Deep sequencing showed that approximately 42–48% of genes underwent alternative splicing (AS) of mRNA in *Arabidopsis* and rice (Filichkin *et al.*, 2010; Lu *et al.*, 2010b). In addition, Qin *et al.* (2017) identified an AS event in *BdFTL1* locus. As such, we explored AS events in the *BdFTL1* and *BdFTL2* loci. Coding DNA sequence (CDS) identification showed that *BdFTL1* was subject to AS under LD conditions (Figure 3d), whereas no AS was observed at the *BdFTL2* locus (Figure 3e). The AS event at *BdFTL1* generated a transcript isoform with a premature stop codon that was predominant for 3 weeks after germination (Figures 3d and S3). This suggested that AS of *BdFTL1* might impair its function in flowering during these early developmental stages.

BdFTL2* influences both transcription and alternative splicing of *BdFTL1

The AS event in *BdFTL1* resulted in the late appearance of the functional transcript, which in WT lines gradually increased to high levels and became predominant 5 weeks after germination (Figure 3d). Therefore, 5-week-old seedlings should possess flowering competency even in a *BdFTL2* loss of function mutant. However, *BdFTL2*-KO lines with a native *BdFTL1* did not flower for ~3 months under inductive LD conditions (Figure 2d,e). We speculated that the functional transcript of *BdFTL1* in *BdFTL2*-KO lines was expressed at lower levels than in WT lines. To test this hypothesis, we firstly compared *BdFTL1* transcriptional levels between *BdFTL2* KO and WT lines. qPCR indicated that *BdFTL1* in *BdFTL2*-KO lines had much lower transcriptional levels than that in WT lines, consistent with the previously published data from the analysis of *BdFTL2* RNAi lines (Figure 3f; Lv *et al.*, 2014). Moreover, due to AS, the *BdFTL1* functional transcript was almost undetectable in *BdFTL2*-KO lines up to 10 weeks after germination (Figure 3g). *BdFTL2* OE could also promote the expression of *BdFTL1* (Figure S4). Thus, *BdFTL2* directly or indirectly regulates the transcriptional activity and AS of *BdFTL1*.

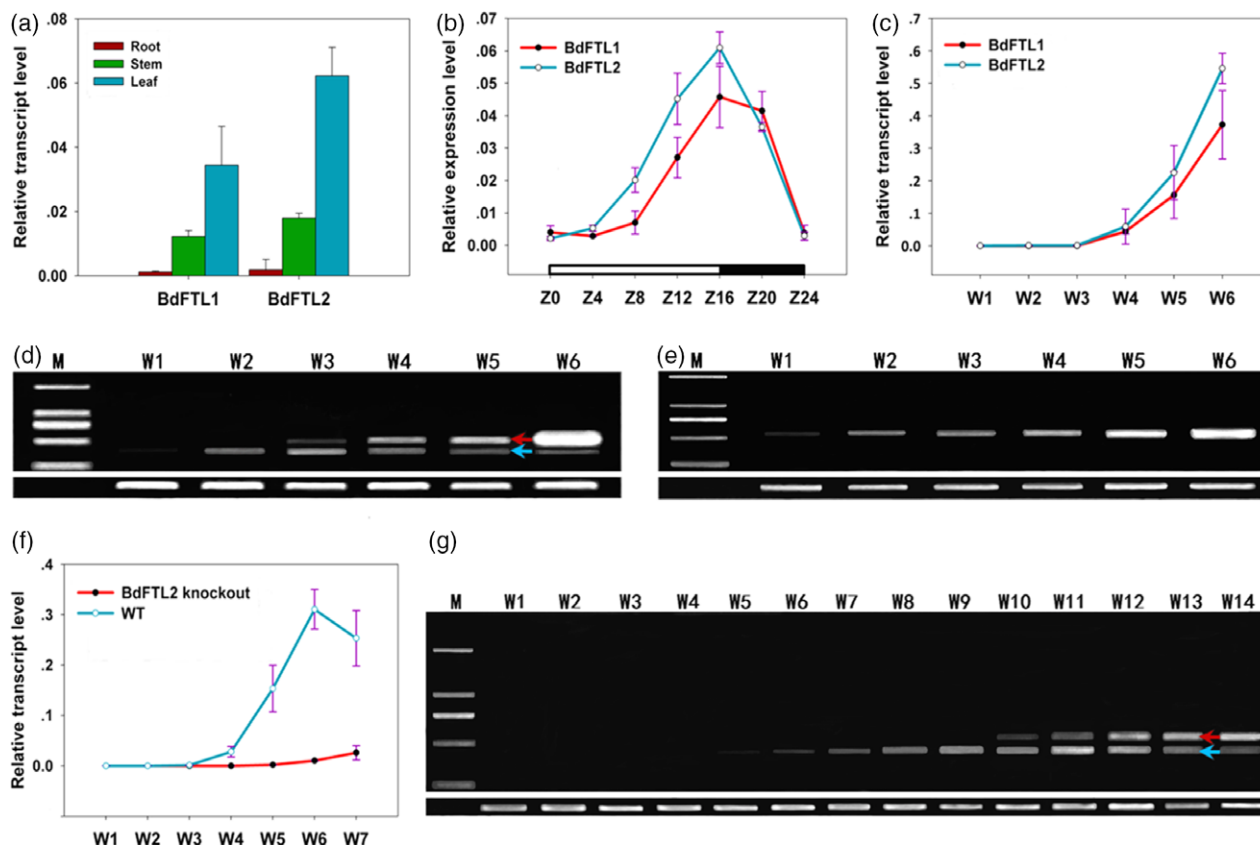


Figure 3. Transcriptional patterns and alternative splicing (AS) events for *BdFTL1* and *BdFTL2* under inductive long-day (LD) conditions.

Transcriptional patterns of *BdFTL1* and *BdFTL2* in (a) tissues of 4-week-old seedlings, (b) a time-course of 1 day for 3rd and 4th leaves of 4-week-old seedlings; Z0 ~ 24: Zeitgeber 0 ~ 24, (c) over 6 weeks; 1- to 6-week-old leaves were used. Paired *t*-tests show that *BdFTL1* and *BdFTL2* have similar tissue-specific expression profiles ($P = 0.0578$ in Table S1), parallel transcriptional patterns during a time-course over a full day ($P = 0.1489$ in Table S1) and consistent transcriptional variation over different developmental phases ($P = 0.7186$ in Table S1).

(d) Detection of AS products from the *BdFTL1* locus under inductive LD conditions during developmental processes. Samples were the same as those used in (c). Red and blue arrows show the functional transcript with the complete coding DNA sequence (CDS; its function to promote flowering was identified by over-expression experiments in Figure 2a) and the AS-derived isoform with a premature stop codon, respectively. M: DL2000 DNA marker (Takara) including DNA fragments of 2000, 1000, 750, 500 and 250 bp (from top to bottom). The bands in the lower part of this panel are the target fragment amplified from *BdUBC18*, which acted as an internal reference to calibrate the expression level of *BdFTL1*.

(e) No AS event was observed at the *BdFTL2* locus. Here the samples, marker and internal gene were the same as those in (d).

(f) Transcriptional patterns of *BdFTL1* in 1- to 7-week-old leaves from WT and *BdFTL2*-KO lines, respectively. The quantitative polymerase chain reaction (qPCR) curve showed the total transcription pattern of all splicing variants.

(g) Transcriptional activities and AS events 1- to 14-week-old leaves of *BdFTL1* in *BdFTL2*-KO lines under inductive LD conditions during plant development. Red and blue arrows, the samples, marker and internal gene were the same as those in (d).

BdFTL2 interacts with BdES43, an H3K4me3 reader

Because *BdFTL2* greatly affects *BdFTL1* transcriptional activity and AS, we further investigated the potential role of *BdFTL2* in regulating *BdFTL1*. Previous research showed that FT usually regulates downstream targets by binding other proteins such as FD-like and 14-3-3-like proteins (Taoka et al., 2013). To identify proteins interacting with *BdFTL2*, we performed yeast-two-hybrid (Y2H) screens using a previously constructed *Brachypodium* Y2H library (Cao et al., 2011b). Six representative partners of *BdFTL2* were identified, including a previously identified mtN19 homolog (Adrian, 2009), and new partners BdES43, Bd2OG, BdSTN7, BdB2 and BdDUF886 (Figure 4a;

Table S2). However, we did not isolate the expected FD-like and 14-3-3-like proteins as partners of *BdFTL2* in this library screen. The Y2H library used in this study was constructed from 2-week-old seedlings (Cao et al., 2011b), and transcriptional analyses showed that *BdFDL2* and *Bd14-3-3B* had very low transcriptional levels in 2-week-old shoot tissues (Figure S5a), which might account for why they were not identified as interactors in the screen. Therefore, we additionally isolated the four 14-3-3 and two FD homologs in *Brachypodium* based on previous reports in wheat (Li and Dubcovsky, 2008; Li et al., 2015) and directly tested their potential interactions with *BdFTL2* by Y2H; only *BdFDL2* and *Bd14-3-3B* were observed to bind with *BdFTL2* (Figure S5b).

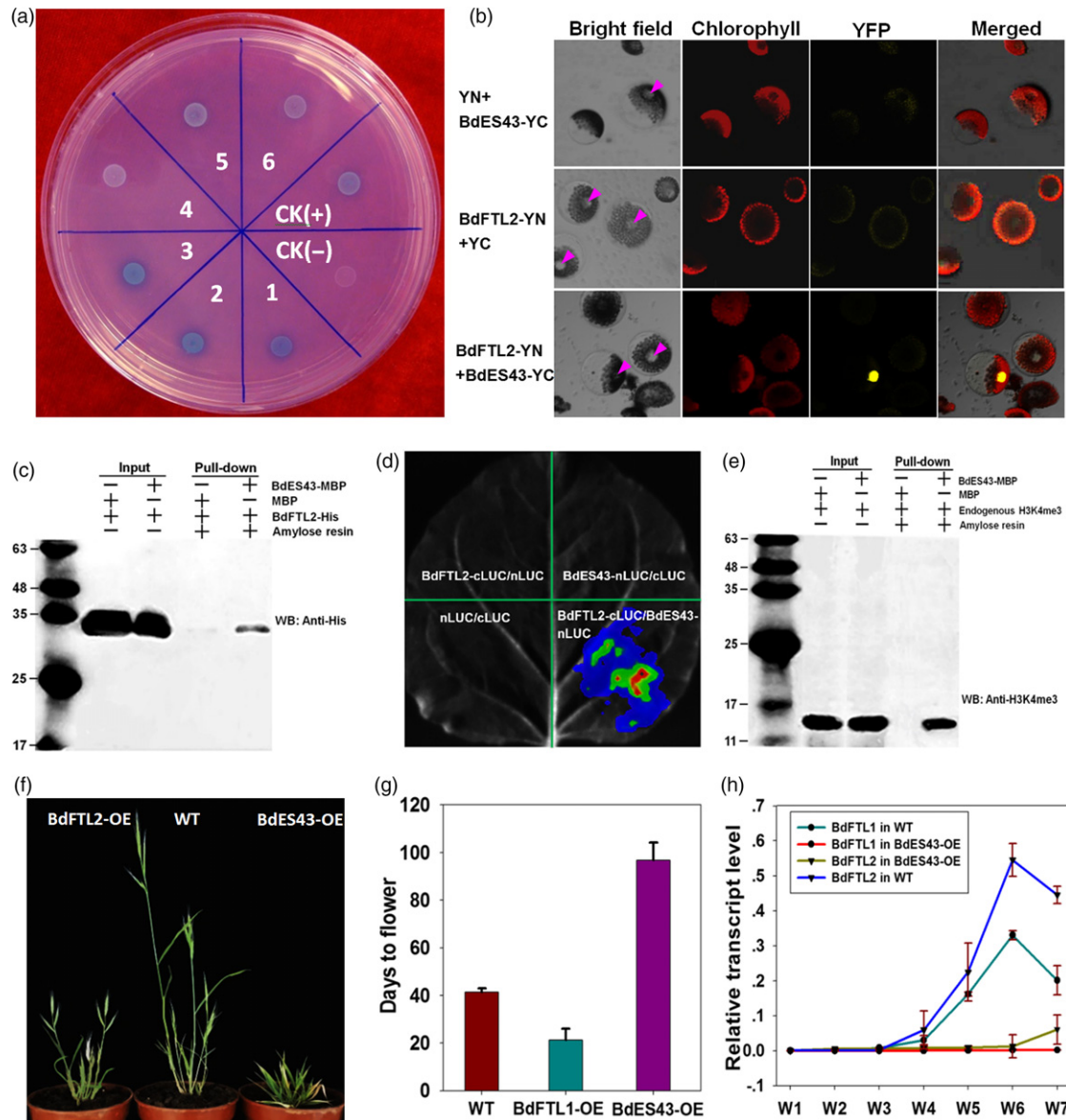


Figure 4. BDFTL2 interacts with BdES43 in targeting H3K4me3.

(a) Interacting BDFTL2 partners identified by yeast-two-hybrid (Y2H) screens; 1: BdmtN19 (Bradi3g41600), 2: BdES43 (Bradi1g55090), 3: Bd2OG (Bradi1g51390), 4: BdSTN7 (Bradi2g17660), 5: BdB2 (Bradi2g40870), 6: BdUPF06870 (Bradi2g41340). CK(+) and CK(-) represent the manufacturer's (Invitrogen) positive and negative controls, respectively. These partners of BDFTL2 identified from yeast-two-hybrid (Y2H) screening are retested to confirm their interaction with BDFTL2 in yeast.

(b) Bimolecular fluorescence complementation (BiFC) experiments to investigate interaction of BDFTL2 and BdES43 in *Brachypodium* protoplasts. YC + BDFTL2-YN and YN + BdES43-YC are negative controls (NC). Compared with NC, BDFTL2-YN + BdES43-YC can generate observable signals in the nuclei of the protoplasts, showing they can interact in *Brachypodium* protoplasts. Pink arrows show the location of nuclei in bright fields.

(c) Pull-down assays to validate physical interaction between BDFTL2 and BdES43. M: protein marker (GenStar, M221-05). BDFTL2 and BdES43 were fused with His and MBP tags, respectively, and expressed in *Escherichia coli*. Amylose resin was used as an affinity matrix to isolate the proteins fused to maltose-binding protein (MBP). The interaction of BDFTL2 and BdES43 *in vitro* was detected by Western blot with His antibody.

(d) Luciferase complementation (LUC) experiments in tobacco to confirm the interaction between BDFTL2 and BdES43. The regions infiltrated with BDFTL2-cLUC/nLUC, BdES43-nLUC/cLUC or nLUC/cLUC were NC. No signal was detected in the NC regions, while signals could be observed in the region infiltrated with BDFTL2-cLUC/BdES43-cLUC, showing they can bind *in planta*.

(e) Pull-down assays to validate interaction between BdES43 and H3K4me3. BdES43 were fused with MBP tag and expressed in *E. coli*. As the H3K4me3 input, nuclear proteins were extracted from 3-week-old seedlings. Western blot detected by H3K4me3 antibody showed that BdES43 could bind H3K4me3 *in vitro*.

(f) Phenotypic traits of 35S-driven *BdES43*-OE lines. The representative plants for WT, *BdFTL2* OE and *BdES43* OE are 45, 25 and 45 days old, respectively, post-seed germination.

(g) Days to flowering of WT, *BdFTL2* OE and *BdES43* OE lines.

(h) Comparison of *BdFTL1* and *BdFTL2* transcription patterns between WT and *BdES43*-OE lines under inductive LD conditions during developmental processes; 1–7 week-old leaves are used.

Interestingly, among the newly isolated partners of BdFTL2, BdES43 contains bromo-adjacent homology (BAH) and plant homeodomain Zn finger (PHD) domains (Figure S6a). The PHD domain is thought to mediate protein–protein interactions, and usually appears in transcriptional regulators involved in chromatin remodeling (Wysocka *et al.*, 2006; de la Paz Sanchez and Gutierrez, 2009; López-González *et al.*, 2014; Qian *et al.*, 2018). Alignment and homology analyses showed that BdES43 was highly similar to AtEBS and AtSHL, especially in functionally important amino acid residues of the BAH and PHD domains, recognizing H3K27me3 and H3K4me3, respectively (Figure S6a–c; Qian *et al.*, 2018). Bimolecular fluorescence complementation (BiFC), pull-down and luciferase complementation (LUC) experiments all confirmed interactions between BdFTL2 and BdES43 (Figure 4b–d). Pull-down assays validated that BdES43 could bind with native H3K4me3 extracted from *Brachypodium* seedlings, but hardly interacted with H3K27me3 (Figures 4e and S7), which is consistent with the previously reported result in López-González *et al.* (2014). Moreover, BdES43-OE resulted in late flowering and a dwarf stature under inductive LD conditions (Figure 4f). H3K4me3 is also known to be associated with transcriptional regulation and AS (Spies *et al.*, 2009; Tian *et al.*, 2011; Ding *et al.*, 2012; Huang *et al.*, 2012; Davie *et al.*, 2016). Thus, these data suggest that the BdFTL2 regulation of BdFTL1 may be mediated by interactions with the BdES43-H3K4me3 complex.

BdES43 and BdFTL2 have opposite transcription patterns in flower initiation

BdFTL2-OE greatly promoted flowering, whereas BdES43-OE caused extremely late flowering (Figure 4f). Additionally, BdFTL2 could physically bind with BdES43 (Figure 4b–d), suggesting their respective functions in flowering are coupled through their physical interaction. To probe the genetic relationship of BdFTL2 and BdES43 in flowering, their expression patterns in different background lines were additionally investigated and compared. We observed that BdFTL2 transcription in WT lines increased with developmental progress, as in the experiments above (Figure 3c), whereas BdES43 expression was constitutively highly expressed in leaves throughout development (Figure S6e). Accordingly, the WT line gradually gained flowering capacity with developmental progress and flowered at the expected phase. In the BdFTL2-OE lines, plants flowered early while BdES43 retained its normal constitutive expression (Figures 2a and S6f). In the converse experiment, BdES43-OE plants flowered extremely late and have significantly reduced BdFTL2 expression compared with the WT line (Figures 4f,g and S6g). Thus, the delayed flowering of BdES43-OE is likely resulted from the reduced levels of BdFTL2 transcription during the first 8–9 weeks post-seed germination. These findings verified that BdFTL2

and BdES43 have antagonistic effects on flowering initiation and determine flowering in a transcription-dependent manner.

BdES43 affects BdFTL1 expression

Because BdFTL2 can alter BdFTL1 expression, likely through its interaction with BdES43, it is necessary to investigate the BdFTL1 expression pattern in BdES43-OE lines. Transcriptional pattern assays in BdES43-OE lines showed that BdFTL1 transcripts were barely detectable for 7 weeks post-germination, and its AS-derived transcripts were predominant up to 9 weeks after germination (Figures 4g and S6d). Thus, BdES43 alterations had an obvious effect on transcription and AS of BdFTL1. Chromatin immunoprecipitation (ChIP)-qPCR assays also showed BdES43 and H3K4me3 had similar distribution patterns at the BdFTL1 locus: higher affinity with the promoter and AS region than with the more downstream regions of the BdFTL1 locus (Figure 5a,b; Table S3). Our data collectively suggested that BdES43 might regulate the transcription and AS of BdFTL1 by interacting with H3K4me3.

BdFTL2, BdES43 and H3K4me3 have similar enrichment patterns in the BdFTL1 locus

To further investigate whether BdFTL2 can bind the BdFTL1 locus, ChIP experiments were performed using BdFTL2-OE lines. ChIP-qPCR assays showed that BdFTL2 and H3K4me3 physically bind to similar regions of the BdFTL1 locus, consistent with that of BdES43 (Figure 5a–c; Table S3). We also detected the presence of H3K4me3 at the BdFTL1 locus in the WT lines during different developmental stages. The distributional enrichment of H3K4me3 was higher in the promoter and AS regions than in more distal positions of BdFTL1, and exhibited roughly parallel changes at each site during development (Figure 5d). Therefore, co-localization of BdFTL2, BdES43 and H3K4me3 in the promoter and AS region of BdFTL1, as well as their genetic and physical interactions described above, strongly suggests they synergistically regulate the transcription and AS of BdFTL1. Considering that H3K27me3 is also known to be involved in AS and transcription (Luco *et al.*, 2010; Mercer *et al.*, 2013), we also investigated H3K27me3 distribution within BdFTL1 locus and found that its enrichment in the promoter and around AS site is not significantly higher than that in more distal positions of BdFTL1 (Figure 5b,c,e). Moreover, we compared the distribution of BdES43, H3K27me3 and H3K4me3 within BdFTL2 locus using the 2-week-old leaves of BdES43-OE lines (Figure S8). ChIP-qPCR showed that H3K27me3 enrichment in the promoter of BdFTL2 was significantly higher than other distal regions, whereas H3K4me3 and BdES43 were not. Thus, H3K27me3 may have an effect on the expression of BdFTL2, while H3K4me3 and BdES43 probably are irrelevant with BdFTL2.

DISCUSSION

In the present study, we achieved the functional dissection of *Brachypodium* FT homologs *BdFTL1* and *BdFTL2* by transgenic assays. Although there is no statistically

significant difference in flowering time between *BdFTL1* KO and WT lines, *BdFTL1* KO delayed flowering for more than 5 days compared with WT (Dataset S3). Additionally, *BdFTL1* OE can greatly accelerate flowering just as *BdFTL2*. Furthermore, *BdFTL1* is subject to AS in WT lines, probably

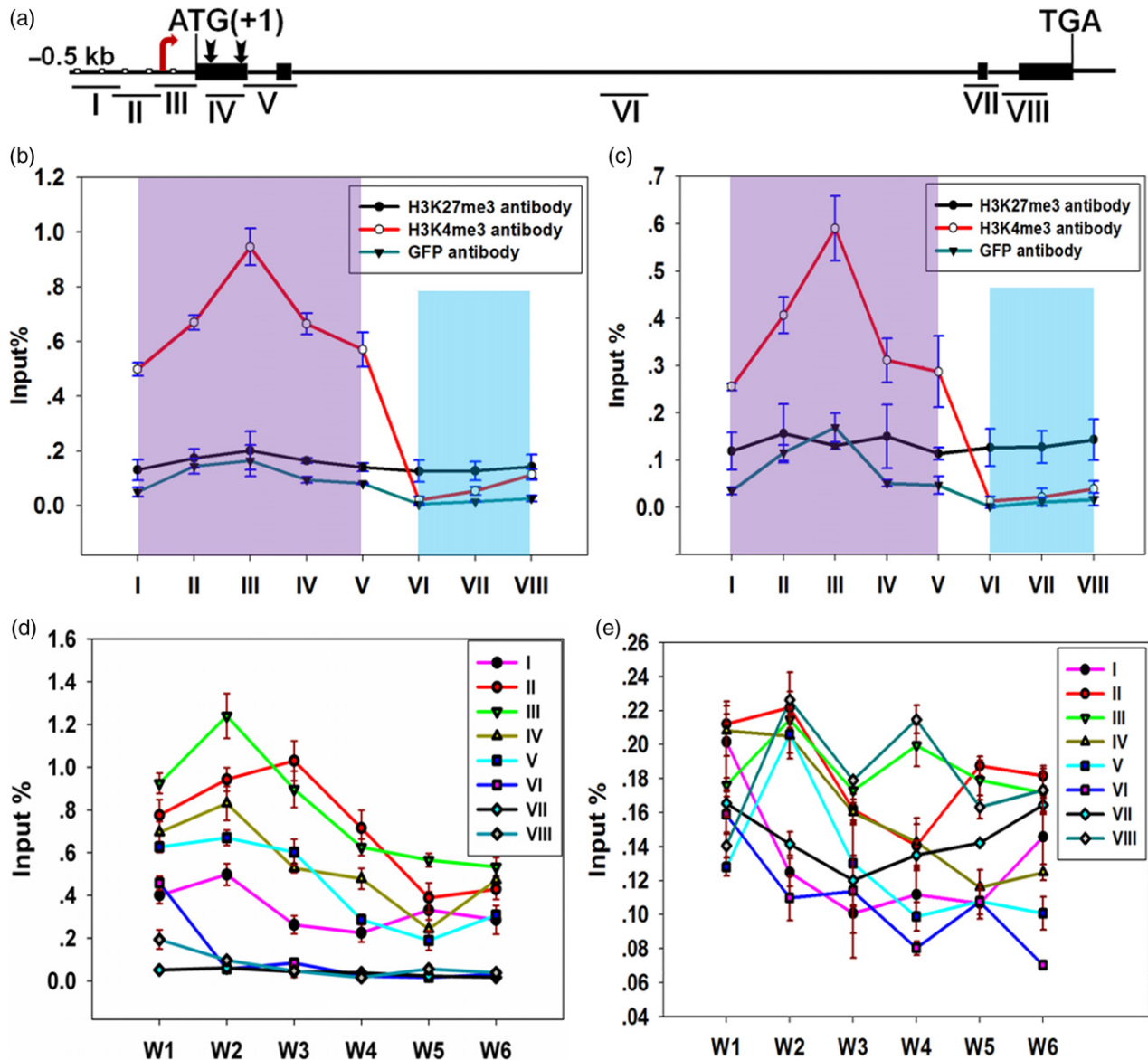


Figure 5. *BdFTL2* regulates *BdFTL1* by binding with the *BdES43*-H3K4me3 complex.

(a) Schematic of the *BdFTL1* locus showing primer-targeted sites for chromatin immunoprecipitation (ChIP)-quantitative polymerase chain reaction (qPCR) experiments. The downward arrows show the alternative splicing (AS) site and the red right arrow indicates the location of the transcriptional start site (TSS). The TSS is located at approximately 146 bp upstream to the start codon ATG and is predicted using TSSP (<http://www.softberry.com/berry.phtml?topic=tsspa&ndgroup=programs&subgroup=promoter>). The black rectangles and black lines show the exons and introns, respectively. The black lines with white dots indicate the promoter of *BdFTL1* and the distance between two adjacent dots is 100 bp.

(b) H3K4me3 H3K27me3 and *BdES43* distributions within the *BdFTL1* locus. The promoter plus AS region (represented by I, II, III, IV and V regions) and more distal locations (represented by VI, VII and VIII regions) of *BdFTL1* locus were highlighted in pink and blue, respectively. The 2-week-old seedlings of *BdES43*-OE lines were used.

(c) H3K4me3 H3K27me3 and *BdFTL2* distribution within the *BdFTL1* locus of *BdFTL2*-OE lines. The promoter plus AS region (represented by I, II, III, IV and V regions) and more distal locations (represented by VI, VII and VIII regions) of *BdFTL1* locus were highlighted in pink and blue, respectively. The 2-week-old seedlings of *BdFTL2*-OE lines were used.

(d) H3K4me3 distribution within the *BdFTL1* locus of WT lines at different stages of development.

(e) H3K27me3 distribution within *BdFTL1* locus of WT line at different stages of development.

accounting for the comparable flowering time between its KO and WT lines. Collectively, *BdFTL1* is a promoter of flowering just as *BdFTL2*, and its function in accelerating flowering may be impaired by the AS event. We found that *BdFTL2* has a significant effect on AS and transcription activity of *BdFTL1* through transgenic KO and OE experiments (Figure 3g). Most importantly, we uncovered that *BdFTL2* can bind to BdES43, and BdES43 can also interact with H3K4me3. *BdFTL2* and *BdES43* have opposite effects on the transcriptional initiation of *BdFTL1* and flowering. Additionally, *BdFTL2*, *BdES43* and H3K4me3 successively interact and have similar distribution patterns at the *BdFTL1* locus: higher enrichment in the promoter and AS regions than in more distal positions (Figure 5a–d). Thus, it is of biological significance to reveal the regulatory mechanism underlying *BdFTL1* for the flowering control in *Brachypodium*.

Evidence for coupling between transcriptional and splicing machinery is rapidly accumulating, especially for genes with long introns that may severely reduce the transcription elongation rate and increase AS efficiency (Bell *et al.*, 1998; Hatton *et al.*, 1998; Burnette *et al.*, 2005; Fox-Walsh *et al.*, 2005; Graveley, 2005; Kim *et al.*, 2006; McGuire, 2008; Roy *et al.*, 2008; Kandul and Noor, 2009; Pandya-Jones and Black, 2009; Spies *et al.*, 2009; Shukla and Oberdoerffer, 2012). Most published splicing events of constitutive exons also are co-transcriptional in a general 5' to 3' order, i.e. the closer the splicing site is to the 5' terminal region of a gene, the higher the possibility that AS couples with the transcription process (Pandya-Jones and Black, 2009). The target AS site of *BdFTL1* lies in the first exon, followed by a long downstream intron (Figure S3). We thus speculate that the AS of *BdFTL1* is co-transcriptional. Considerable evidence has revealed that transcription elongation rates are tightly related to chromatin structure and directly involved in the AS events in co-transcriptional splicing processes (Shukla and Oberdoerffer, 2012; Braunschweig *et al.*, 2013; Kornblihtt *et al.*, 2013; Bentley, 2014). Moreover, it is well known that H3K4 methylation exerts a significant influence on gene transcription and AS (Burnette *et al.*, 2005; Spies *et al.*, 2009; Tian *et al.*, 2011; Ding *et al.*, 2012; Huang *et al.*, 2012; Ong-Abdullah *et al.*, 2015; Davie *et al.*, 2016). Here we present a model for *BdFTL2* regulation of *BdFTL1* based on our experimental evidence and above reasoning (Figure 6a). According to our model, a BdES43 complex binds with H3K4me3 in the early plant developmental phases to repress transcription initiation and elongation rates at the *BdFTL1* locus by chromatin remodeling. The elongation rate is so slow that long dwell times for coupling transcription and splicing in the target splicing site promote the occurrence of AS of *BdFTL1*. Consequently, the transcriptional efficiency of *BdFTL1* is low and AS occurs frequently in the early growth stages. As development proceeds, *BdFTL2* expression increases and influences the function of

the BdES43 complex through their interaction. As a result, the interaction triggers the derepression of *BdFTL1* transcription and a concomitant reduction in AS.

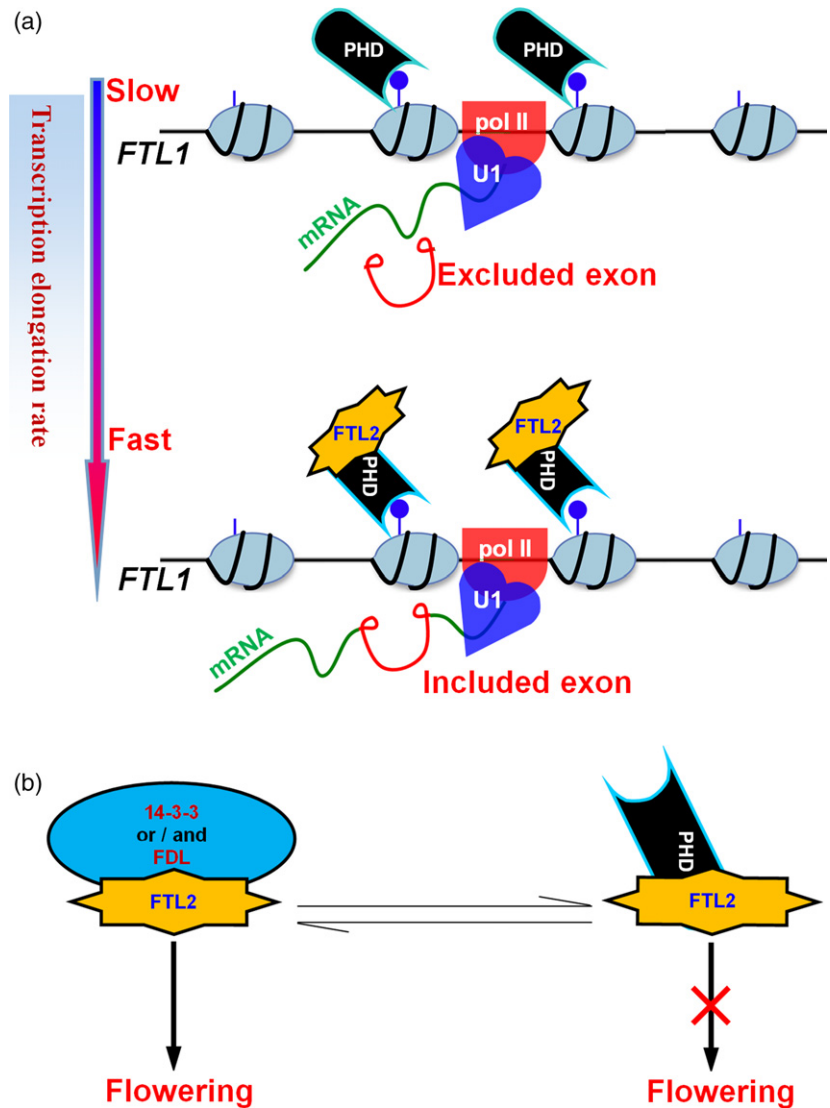
In this study, the interaction between *BdFTL2* and BdES43 plays the central role in tracking how *BdFTL2* regulates *BdFTL1*. It has been proposed in the model above that *BdFTL2* modulates the structure of the BdES43 complex and alters its function. Conversely, BdES43 should also affect the function of *BdFTL2* concurrently. We achieved *BdFTL2*-OE in the *BdFTL1*-KO background (*BdFTL2*-OE/*BdFTL1*-KO) through hybridization of *BdFTL2*-OE and *BdFTL1*-KO lines. The *BdFTL2*-OE/*BdFTL1*-KO lines flowered a little later than *BdFTL2*-OE in WT lines, and much earlier than *BdFTL1*-KO and WT lines (Figure S9), suggesting that *BdFTL2* partially regulates flowering via *BdFTL1* regulation. Additionally, *BdFTL2* might form a flowering-activating complex by interacting with *Brachypodium* 14-3-3 and FD homologs (Figure S5b), indicating that *BdFTL2* controls flowering through multiple molecular regulatory pathways. Recently, it was shown that the OE of a *BdFTL1* splice transcript repressed flowering by preventing the assembly of a functional flowering-activating complex containing *BdFTL1*, *BdFTL2*, 14-3-3 and FD proteins, providing additional cues to their relationships in flowering initiation (Qin *et al.*, 2017). It is thus possible that BdES43 sequesters *BdFTL2* from the flowering-activating complex to cause late flowering. We speculated that the competitive binding of BdES43 and the homologs of FD and/or 14-3-3 with *BdFTL1* may be an important cause of extremely late flowering of *BdES43*-OE lines (Figure 6b). In the near future, we will test the hypothesis through protein competitive interaction (e.g. yeast-three-hybrid or pull-down methods) and transgenic assays.

AtEBS and AtSHL, homologs of BdES43, interact genetically with numerous flowering-related epigenetic modifiers, such as HDACs with deacetylase activity, ATX1/ATXR7 with putative Set 1 class H3K4 methylase activity, and EFL6 and HUMONJ14/14(JMJ4/JMJ14) with demethylase activity (Tamada *et al.*, 2009; Lu *et al.*, 2010a; Yu *et al.*, 2011; He, 2012; Yang *et al.*, 2012; López-González *et al.*, 2014). Additionally, there is evidence that AtEBS can bind physically with the HDAC family members, HDA6 and HDA19 (López-González *et al.*, 2014). A number of other PHD proteins have also been shown to control gene expression by recognizing H3K4me3 and recruiting epigenetic factors that can activate or repress the transcription of underlying genes (Shi *et al.*, 2006; Wysocka *et al.*, 2006; de la Sanchez and Gutierrez, 2009; He, 2012; Rincon-Arango *et al.*, 2012; Molitor *et al.*, 2014). Therefore, there is every reason to believe that *BdFTL2* affects the BdES43 complex by recruiting chromatin-remodeling factors. As such, it is conceivable that *BdFTL2*-BdES43-H3K4me3 in the nucleosome is not only a structural unit, but also a signaling platform. Further experiments are necessary to address this question.

Figure 6. Flowering regulatory models underlying BdES43 interaction with BdFTL2.

(a) The working model of BdFTL2 regulating *BdFTL1* transcription and alternative splicing (AS) through interacting with BdES43. U1: mRNA splicing complex; pol II: RNA polymerase II transcription complex. *FTL1*: *BdFTL1* locus; FTL2: BdFTL2 protein; PHD: BdES43 protein.

(b) The working model of BdES43 vying with BdFDL and/or Bd14-3-3 members for BdFTL2 to regulate flowering time. FDL: BdFDL protein; 14-3-3: Bd14-3-3 protein.



In addition to flowering, FT has also been identified as a major regulatory factor in a wide range of developmental processes, including fruit set, vegetative growth, stomatal control and tuberization (Pin and Nilsson, 2012; Navarro *et al.*, 2015). Here we revealed that the FT ortholog BdFTL2 is involved in chromatin remodeling. This finding fits well with the known roles for FT in the regulation of different developmental processes, and supplies an additional entry point to explore the molecular basis of its pleiotropic effects.

EXPERIMENTAL PROCEDURES

Plant material, growth conditions and phenotype characterizations

Brachypodium accession Bd21 was supplied kindly by Prof. Ben Holt III of Oklahoma University, and used as the recipient for OE and KO of target genes. Seeds were imbibed overnight in darkness between wet paper towels at room temperature and then

sown in soil. Seedlings were grown in a growth chamber with 16 h of light per day (LD) and light intensity of 150 μ E provided by cool-white tubes. The day/night temperature pattern in the growth chamber was 22/18°C. Flowering time was measured as the number of days from seed germination to heading of the main stem.

Transgenic experiments for overexpression and knockout

Gateway-compatible ZmUbi-driven pGW101-pBI and CaMV35S-driven pEarleyGate101 vectors were used to overexpress genes of interest. The coding sequences of *BdFTL1* and *BdFTL2* for OE experiments are the same as the annotation of Bradi2g07070 and Bradi1g48830, respectively, in BdGDB (<http://plantgdb.org/BdGDB/>). TALEN vector construction and activity assays in protoplasts were performed as previously described (Shan *et al.*, 2013). To construct the TALEN vector, candidate sites were used as queries to perform BLAST against *Brachypodium* genome and were also identified by the TAL EFFECTOR-NUCLEOTIDE TARGETER 2.0 program (<https://talen.cac.cornell.edu/>), which will guarantee that the target sites are unique and of low-identity with other regions (Doyle *et al.*, 2012). TALEN repeat arrays were listed in Dataset S4 and were constructed using the Golden Gate method (Zhang *et al.*, 2013). Each TALEN

recognition sequence contained a restriction enzyme site within the spacer region in favor of identification for applicable constructs and positive lines (Dataset S4). TALEN repeat arrays were cloned into expression vector pZHY051 and then transferred into protoplasts using polyethylene glycol (Zhang *et al.*, 2013). The nuclease activity directed by the resulting constructs was assessed through PCR/RE assays as described in Shan *et al.* (2013). The transformed protoplasts were incubated for 48 h and were used to extract genomic DNA. The PCR products encompassing each target site were digested by restriction enzymes and visualized in agarose gel. The PCR amplicons were then cloned and sequenced to confirm the mutations. *Agrobacterium*-mediated transformation was carried out following a previously described procedure with slight modifications, i.e. longer (15 min) desiccation treatment after inoculation of callus with *Agrobacterium* and coculturing callus with *Agrobacterium* at lower temperature (21°C) to reduce excessive proliferation of *Agrobacterium* (Alves *et al.*, 2009). The target plants were identified by PCR/RE assays just as described above. The mutant lines were identified with agarose gel electrophoresis and sequencing (Figure S1). To determine whether there are off-target events, the regions with some degree of similarity to the TALEN target site were investigated. In detail, the genes including similar target regions were identified using BLAST in BdGDB (<http://plantgdb.org/BdGDB/>), isolated from the TALENed lines using the gene-specific primer pairs and sequenced to investigate off-target events.

Genomic DNA extraction, total RNA isolation and cDNA synthesis

Three independent plant samples were prepared for each tissue type. Prior to extraction of genomic DNA and total RNA, samples were ground in frozen mortars. DNA and RNA were extracted from *Brachypodium* seedlings using the standard CTAB method and an E.Z.N.A. Plant RNA Kit (Omega Biotek, Cat#R6827, <https://www.omegabiotek.com/>), respectively. Quality and quantity of extracted DNA and RNA from all samples were confirmed by both agarose gel visualization and spectrophotometry (Thermo Scientific, NanoDrop™ 1000, <https://www.thermofisher.com/>). Total RNA samples were pretreated with recombinant DNase I to eliminate any contaminating genomic DNA and then were synthesized into primary cDNA using a PrimeScript™ RT reagent Kit with gDNA Eraser following the manufacturer's instructions (TaKaRa, Cat#RR047A, <https://www.takarabio.com/>).

Identification of mRNA alternative splicing events with reverse transcription-polymerase chain reaction

To identify mRNA AS in *BdFTL1* and *BdFTL2* loci, reverse transcription (RT)-PCR was used to amplify their full-length CDS using the primer pairs, *BdFTL1*-CDS-F1/R1 and *BdFTL2*-CDS-F1/R1 (Table S4). RT-PCR was also used to isolate the complete CDS of *BdES43*. RT-PCR was performed in 25 µl reaction volumes comprising 2 µl of each primer (5 µM), 12.5 µl 2 × PCR Mix (Xinhuitian Biotechnology, Cat#HT201, <http://www.ht-biotech.net/>), and 2.5 µl cDNA. PCR conditions were: 1 min at 94°C, followed by 30 cycles of 10 sec at 94°C, 20 sec at 65°C, and 0.5 or 1 min at 72°C, with a final extension of 5 min at 72°C. PCR products were resolved by electrophoresis in 1 or 2% agarose gels, visualized using ethidium bromide staining, and photographed with the BioRad imaging system.

Quantitative real-time reverse transcription-polymerase chain reaction

The relative standard curve method was used when performing quantitative real-time RT-PCR (qPCR) experiments to obtain

transcription patterns for genes of interest (Cao *et al.*, 2011a). An ubiquitin-conjugating enzyme (*BdUBC18*, accession number: Bra di4g00660) in *Brachypodium* was a uniformly expressed control gene to calibrate the expression level of the genes of interest. A series of diluted genomic DNA was used to construct standard curves and calibrate PCR efficiencies. *BdFTL1*, *BdFTL2* and *BdES43* expression analyses were performed on cDNA samples collected from three biological replicates using the CFX Connect™ Real-Time System (Bio-Rad, <http://www.bio-rad.com>). Each primer pair spanned at least one intron to eliminate interference from genomic DNA. Each 25 µl qPCR mix included 12.5 µl SYBR Master Mix (Fermentas, Cat#K0223, <https://www.thermofisher.com/>), 2.5 µl primer pair mix (2 µM for each primer) and 5 µl gDNA (gradient from 100 to 0.032 ng µl⁻¹ with a dilution factor of 5 for the standard curve) or cDNA as templates. Transcriptional patterns of *BdFTL1* and *BdFTL2* in the tissues of 4-week-old seedlings including roots, shoots and leaves, a time-course (0, 4, 8, 12, 16, 20 and 24 h) of 1 day for the third and fourth leaves of 4-week-old seedlings, and leaves of 1 to 6-week-old seedlings were investigated.

Yeast-two-hybrid screen, bimolecular fluorescence complementation and pull-down assays

The full-length coding region of *BdFTL2* (Bradi1G48830) was directionally cloned into the Gateway™ entry vector pENTR™-D-TOPO® as described by the manufacturer, and then shuttled into the destination vector pDEST32 using LR reaction (Invitrogen, Cat#K2400-20, <https://www.thermofisher.com/cn/zh/home/brands/invitrogen.html>). The Y2H screen was performed using the Gateway cDNA libraries constructed previously (Cao *et al.*, 2011b). The partners (named 'prey') of the protein of interest (named 'bait') identified from Y2H library screening usually are retested to confirm their interaction. The 'prey' vector of the partners was isolated and then re-transformed with the 'bait' vector into yeast. BiFC experiments were carried out using the toolkit reported previously (Waadt *et al.*, 2008). Full-length *BdFTL2* and *BdES43* were fused into pUC-SPYNE(R)173 and pUC-SPYCE(M), respectively. The resulting plasmids were co-transformed into *Brachypodium* protoplasts following the previously described procedure (Rincon-Arango *et al.*, 2012). A confocal microscope was used to capture interaction signals following the procedure and parameter setting for YFP provided in the manufacturer's tutorial manual (Zeiss LSM700, <https://www.zeiss.com/corporate/int/home.html>). The fluorescence can be emitted from excited chlorophyll just like YFP. Although the chlorophyll and YFP have different optimal excitation spectrums, 543 and 477 nm, respectively, the spectrum of 477 nm still can excite chlorophyll to emit, albeit weak, fluorescence. To exclude the interruption of chlorophyll, excitation spectrum of 543 nm was used to show the subcellular location of chloroplasts in wheat cells.

Luciferase complementation assays also were used to validate the interaction between *BdFTL2* and *BdES43* as described previously (Chen *et al.*, 2008; Song *et al.*, 2011; Sun *et al.*, 2013). Full-length coding regions of *BdFTL2* and *BdES43* were fused into pCambia1300nLUC and pCambia1300cLUC vectors, respectively. An *Agrobacterium tumefaciens* strain (GV3101) containing the resultant constructs was used to infiltrate *Nicotiana benthamiana* leaves. Luciferase activities in the leaves were determined 50 h after infiltration. Fluorescence was monitored and imaged by LB985 NightSHADE (Berthold Technologies, <http://berthold-us.com/bio-analytical2.html>) shortly after 100 µl of Luciferase assay substrate (Promega, Cat#E1500, <https://www.promega.com.cn/>) was sprayed onto the infiltrated leaves.

For pull-down assays, *BdFTL2* and *BdES43* were fused with His and MBP tags, respectively, and expressed in *Escherichia coli*.

MBP is a natural affinity tag of amylose resin. As the H3K4me3 and H3K27me3 inputs, nuclear proteins were extracted from 3-week-old seedlings. Two grams of each tissue sample was ground into fine powder and then suspended in 10 ml of cold protein extraction buffer A [10 mM Hepes (pH 7.9), 10 mM KCl, 0.2 mM EDTA, 1.5 mM MgCl₂, 1% N-40, 1 mM DTT and 5% glycerol freshly mixed with 1 mM phenylmethylsulfonyl fluoride (PMSF), 3 mg L⁻¹ aprotinin, 3 mg L⁻¹ leupeptin and 2 mg L⁻¹ pepstatin A]. The mixture including the fine powder of tissue samples and the above buffer A was incubated on ice for 15 min and then centrifuged at 2800 *g* for 10 min. The supernatant was discarded and the precipitant was resuspended in 500 µl protein extraction buffer B [20 mM Hepes (pH 7.9), 420 mM KCl, 0.5 mM EDTA, 5 mM MgCl₂, 1% N-40, 1 mM DTT, and 10% glycerol freshly mixed with 1 mM PMSF, 3 mg L⁻¹ aprotinin, 3 mg L⁻¹ leupeptin and 2 mg L⁻¹ pepstatin A]. The mixture including the above precipitant and protein extraction buffer B was incubated in ice for 30 min and then centrifuged at 20 000 *g* for 5 min. The supernatant was harvested and incubated on ice. The purified BdES43-MBP was incubated with amylose resin (NEB, Cat#E8021S, <https://international.neb.com/>) at 4°C for 1 h and then mixed with the cold supernatant above or purified BdFTL2-His. The resulting mixtures were shaken gently for 4 h and passed through a column to retain the resulting resin. Finally, the proteins were eluted from the resin. Protein blots were visualized using Immobilion Western Chemiluminescent HRP Substrate (Merck Millipore, Cat#WBKLS0100, <http://www.merckmillipore.com/>) with His antibody (Abbkine, Cat#A02050; <https://www.abbkine.com/>), H3K4me3 antibody (ABCAM, Cat#AB8580, <https://www.abcam.com/>) or H3K27me3 antibody (ABCAM, Cat#AB6147, <https://www.abcam.com/>).

Chromatin immunoprecipitation-quantitative polymerase chain reaction

For ChIP assays, OE lines of *BdES43* and *BdFTL2* were used to investigate the distribution of the target proteins at the target loci. *BdES43* and *BdFTL2* were fused with an YFP tag in the vector pEarleyGate 101. GFP antibody (ABCAM, Cat#AB6556), H3K4me3 antibody (ABCAM, Cat#AB8580, <https://www.abcam.com/>) and H3K27me3 antibody (ABCAM, Cat#AB6147, <https://www.abcam.com/>) are reactive against YFP, H3K4me3 and H3K27me3, respectively. H3K4me3 and H3K27me3 antibodies were also used to detect H3K4me3 and H3K27me3 distributions at the *BdFTL1* locus of WT lines during plant development. Protein A + G Agarose beads without antibody were used as non-immune controls (NICs). Sample preparation and experimental procedures for ChIP-qPCR assays were as described previously (Cao *et al.*, 2014). In detail, 1 g leaf tissue was ground in liquid nitrogen and resuspended by 30 ml nuclear isolation buffer [10 mM HEPES (pH 7.6), 400 mM sucrose, 5 mM KCl, 5 mM MgCl₂, 5 mM EDTA, 1% formaldehyde, 14 mM 2-mercaptoethanol, 0.6% Triton X-100 and 0.4 mM PMSF]. The lysate was crosslinked at room temperature for 10 min and was stopped by adding 2 ml Glycine (2 M). The lysate was filtered with the filter into a fresh tube. The nuclei was pelleted by centrifuging the filtrate at 2800 *g* for 10 min and dissolved in 200 µl nuclear lysis buffer [50 mM Tris-HCl pH 7.5, 1% sodium dodecyl sulfate (SDS), 10 mM EDTA (pH 8.0)]. The nuclei extract was loaded into a sonicator (Bioruptor UCD200) and sonicated at the program of 30 sec on/60 sec off for five times. The sheared chromatin was centrifuged at 16 000 *g* for 5 min and the supernatant was transferred to a fresh tube. Subsequently, 30 µl protein A + G magnetic beads (Merck Millipore, Cat#16-663, <https://www.merckmillipore.com/>) together with 2 µg target antibody or IgG antibody (NIC) as the negative control were added to the tube, and the mixture was rocked at 4°C overnight. After

incubation, the beads were successively washed by 1 ml low-salt immune complex wash buffer [0.1% SDS, 1.0% Triton X-100, 2 mM EDTA, 20 mM Tris-HCl (pH 8.0), 150 mM NaCl], 1 ml high-salt immune complex wash buffer [0.1% SDS, 1.0% Triton X-100, 2 mM EDTA, 20 mM Tris-HCl (pH 8.0), 500 mM NaCl], 1 ml LiCl immune complex wash buffer [0.25 M LiCl, 1.0% NP-40, 1% sodium dodecyl sulfate, 1 mM EDTA, 10 mM Tris-HCl (pH 8.0)] and 1 ml TE, and eluted by 200 µl elution buffer (1% SDS, 100 mM NaHCO₃). The eluted immune complex was successively incubated at 65°C overnight together with 8 µl NaCl (5 M), and at 50°C for 2 h with 1 µl proteinase (Fermentas, Cat#EO049, <https://www.thermofisher.com/>). The relative standard curve method was employed to test the enrichment of the target proteins at the target loci. Each 25 µl qPCR mix included 12.5 µl of SYBR Master Mix (Fermentas, Cat#K0223, <https://www.thermofisher.com/>), 2.5 µl of primer pair mix (2 µM for each primer) and 5 µl gDNA (gradient from 100 to 0.032 ng µl⁻¹ with a dilution factor of 5 for the standard curve) or ChIPed DNA as templates. The qPCR profile was 2 min at 50°C and 10 min at 95°C, 45 cycles of 10 sec at 95°C, and 1 min at 60°C followed by the default dissociation step for melt curves. All primers are listed in Table S4.

Statistical analyses

The mean values and error bars were calculated with the Excel functions 'AVERAGE' and 'STDEV', respectively. Significant difference was determined by paired *t*-test using SIGMAPLOT 10. Multiple comparison analyses were conducted by Univariate Analysis of Variance (UNIANOVA) in the general linear model using SPSS19. For multiple comparison of each gene, items for comparison were set as fixed factors and the underlying phenotypic data were used as independent variables. In the 'post hoc' menu, the least significant difference algorithm was selected to calculate statistical parameters for comparison.

ACKNOWLEDGEMENTS

We are grateful to Prof. R.A. McIntosh, Plant Breeding Institute, University of Sydney, for critical review of this manuscript. This work was supported by the Natural Science Foundation of China (91935304 and 31571663), National Key R&D program of China (2016YFD0100502) and the Gene Transformation Project (2016ZX08009003-004). [Correction added on 3 March 2020, after first online publication: a typesetting error caused the Author Contributions text to be repeated in the Acknowledgements section, and this has been corrected.]

AUTHOR CONTRIBUTIONS

SC conceived the project and supervised this study. SC, LX and XL performed most of the experiments; CG participated in the material preparation and generation the transgenic lines; SC, DW, BH, HL, CC and XX wrote the paper. All the authors discussed the results and commented on the manuscript.

CONFLICT OF INTEREST

The authors declare that they have no conflict of interest.

DATA AVAILABILITY STATEMENT

Sequence data from this article can be found in the GenBank/EMBL libraries under the following accession numbers: *BdFTL1* (Bradi2g07070), *BdFTL2* (Bradi1g48830), *BdES43* (Bradi1g55090), *BdmtN19* (Bradi3g41600), *Bd2OG*

(Bradi1g51390), BdSTN7 (Bradi2g17660), BdB2 (Bradi2g40870), BdUPF06870 (Bradi2g41340) and BdUBC18 (Bradi4g00660) in BdGDB (<http://plantgdb.org/BdGDB/>).

SUPPORTING INFORMATION

Additional Supporting Information may be found in the online version of this article.

Figure S1. Identification of TALENed *BdFTL1* and *BdFTL2* lines.

Figure S2. Phenotypes of wild-type (WT), *BdFTL1*-knockout (KO) and *BdFTL2*-KO lines under short-day (8 h light/16 h dark) conditions.

Figure S3. Open reading frame and AS pattern of *BdFTL1*.

Figure S4. Transcriptional patterns of *BdFTL1* in 1- to 3-week-old leaves from WT and *BdFTL2*-OE lines.

Figure S5. Transcription patterns of *Brachypodium FD* and 14-3-3 members and Y2H identification for the interaction between their encoded proteins and *BdFTL2*.

Figure S6. Sequence analyses of BdES43 homologs and the comparison of transcriptional activities between *BdES43* and *BdFTL2*.

Figure S7. Pull-down assays to investigate the interaction between BdES43 and H3K27me3.

Figure S8. Distribution of H3K4me3, H3K27me3 and BdES43 within *BdFTL2* locus of *BdES43*-OE lines.

Figure S9. Comparison of flowering time for WT, *BdFTL2*-OE, *BdFTL1*-KO and *BdFTL2*-OE/*BdFTL1*-KO lines under inductive LD conditions.

Table S1. Multiple comparisons and paired *t*-test for the spatial-temporal transcriptional activities of *BdFTL1* and *BdFTL2* based on qPCR arrays.

Table S2. Interactors of *BdFTL2* identified from Y2H screening in this study.

Table S3. Multiple comparisons for the enrichment of target proteins at the *BdFTL1* locus based on ChIP-qPCR arrays.

Table S4. Primers used in this study.

Dataset S1. Sequences of the aligned items for FT homologs.

Dataset S2. Syntenic genes around florigenic loci between *Brachypodium* and rice.

Dataset S3. Multiple comparisons for the flowering time of transgenic lines.

Dataset S4. TALEN sites designed for *BdFTL1* and *BdFTL2*.

REFERENCES

- Adrian, J. (2009) Transcriptional control of FLOWERING LOCUS T in *Arabidopsis*. PhD thesis, Max Planck Institute, Köln, Germany.
- Alves, S.C., Worland, B., Thole, V., Snape, J.W., Bevan, M.W. and Vain, P. (2009) A protocol for *Agrobacterium*-mediated transformation of *Brachypodium distachyon* community standard line Bd21. *Nat. Protocol*, **4**(5), 638–649.
- Andres, F. and Coupland, G. (2012) The genetic basis of flowering responses to seasonal cues. *Nat. Rev. Genet.* **13**(9), 627–639.
- Bell, M.V., Cowper, A.E., Lefranc, M.P., Bell, J.I. and Screaton, G.R. (1998) Influence of intron length on alternative splicing of CD44. *Mol. Cell Biol.* **18**(10), 5930–5941.
- Bentley, D.L. (2014) Coupling mRNA processing with transcription in time and space. *Nat. Rev. Genet.* **15**(3), 163–175.
- Bettgenhaeuser, J., Corke, F.M., Opanowicz, M., Green, P., Hernandez-Pinzon, I., Doonan, J.H. and Moscou, M.J. (2017) Natural variation in *Brachypodium* links vernalization and flowering time loci as major flowering determinants. *Plant Physiol.* **173**, 256–268.
- Braunschweig, U., Gueroussov, S., Plocik, A.M., Graveley, B.R. and Blencowe, B.J. (2013) Dynamic integration of splicing within gene regulatory pathways. *Cell*, **152**(6), 1252–1269.
- Brkljacic, J., Grotewold, E., Scholl, R. et al. (2011) *Brachypodium* as a model for the grasses: today and the future. *Plant Physiol.* **157**, 3–13.
- Burnette, J.M., Miyamoto-Sato, E., Schaub, M.A., Conklin, J. and Lopez, A.J. (2005) Subdivision of large introns in *Drosophila* by recursive splicing at nonexonic elements. *Genetics*, **170**(2), 661–674.
- Cao, S.H., Kumimoto, R.W., Siriwardana, C.L., Risinger, J.R. and Holt, B.F. III (2011a) Identification and characterization of NF-Y transcription factor families in the monocot model plant *Brachypodium distachyon*. *PLoS ONE*, **6**(6), e21805.
- Cao, S.H., Siriwardana, C.L., Kumimoto, R.W. and Holt, B.F. III (2011b) Construction of high quality Gateway entry libraries and their application to yeast two-hybrid for the monocot model plant *Brachypodium distachyon*. *BMC Biotechnol.* **11**, 53.
- Cao, S.H., Kumimoto, R.W., Gnesutta, N., Calogero, A.M., Mantovani, R. and Holt, B.F. III (2014) A distal CCAAT/NUCLEAR FACTOR Y complex promotes chromatin looping at the FLOWERING LOCUS T promoter and regulates the timing of flowering in *Arabidopsis*. *Plant Cell*, **26**(3), 1009–1017.
- Chen, H.M., Zou, Y., Shang, Y.L., Lin, H.Q., Wang, Y.J., Cai, R., Tang, X. and Zhou, J.M. (2008) Firefly luciferase complementation imaging assay for protein-protein interactions in plants. *Plant Physiol.* **146**(2), 368–376.
- Christensen, A.H., Sharrock, R.A. and Quail, P.H. (1992) Maize polyubiquitin genes: structure, thermal perturbation of expression and transcript splicing, and promoter activity following transfer to protoplasts by electroporation. *Plant Mol. Biol.* **18**(4), 675–689.
- Corbesier, L., Vincent, C., Jang, S. et al. (2007) FT protein movement contributes to long-distance signaling in floral induction of *Arabidopsis*. *Science*, **316**(5827), 1030–1033.
- Davie, J.R., Xu, W. and Delcuve, G.P. (2016) Histone H3K4 trimethylation: dynamic interplay with pre-mRNA splicing. *Biochem. Cell Biol.* **94**(1), 1–11.
- Ding, Y., Ndamukong, I., Xu, Z.S., Lapko, H., Fromm, M. and Avramova, Z. (2012) ATX1-generated H3K4me3 is required for efficient elongation of transcription, not initiation, at ATX1-regulated genes. *PLoS Genet.* **8**(12), e1003111.
- Doyle, E.L., Booher, N.J., Standage, D.S., Voytas, D.F., Brendel, V.P., Vandyk, J.K. and Bogdanove, A.J. (2012) TAL Effector-Nucleotide Targeter (TALE-NT) 2.0: tools for TAL effector design and target prediction. *Nucleic Acids Res.* **40**, W117–122.
- Filichkin, S.A., Priest, H.D., Givan, S.A., Shen, R., Bryant, D.W., Fox, S.E., Wong, W.K. and Mockler, T.C. (2010) Genome-wide mapping of alternative splicing in *Arabidopsis thaliana*. *Genome Res.* **20**(1), 45–58.
- Fornara, F., de Montaigu, A. and Coupland, G. (2010) SnapShot: Control of flowering in *Arabidopsis*. *Cell*, **141**(3), 550–550.e552.
- Fox-Walsh, K.L., Dou, Y., Lam, B.J., Hung, S.P., Baldi, P.F. and Hertel, K.J. (2005) The architecture of pre-mRNAs affects mechanisms of splice-site pairing. *Proc. Natl Acad. Sci. USA*, **102**(45), 16 176–16 181.
- Graveley, B.R. (2005) Mutually exclusive splicing of the insect Dscam pre-mRNA directed by competing intronic RNA secondary structures. *Cell*, **123**(1), 65–73.
- Hatton, A.R., Subramaniam, V. and Lopez, A.J. (1998) Generation of alternative Ultrabithorax isoforms and stepwise removal of a large intron by resplicing at exon-exon junctions. *Mol. Cell* **2**(6), 787–796.
- He, Y. (2012) Chromatin regulation of flowering. *Trends Plant Sci.* **17**(9), 556–562.
- Higgins, J.A., Bailey, P.C. and Laurie, D.A. (2010) Comparative genomics of flowering time pathways using *Brachypodium distachyon* as a model for the temperate grasses. *PLoS ONE*, **5**(4), e10065.
- Huang, Y., Min, S., Lui, Y. et al. (2012) Global mapping of H3K4me3 and H3K27me3 reveals chromatin state-based regulation of human monocyte-derived dendritic cells in different environments. *Genes Immun.* **13**(4), 311–320.
- International Brachypodium Initiative (IBI) (2010) Genome sequencing and analysis of the model grass *Brachypodium distachyon*. *Nature*, **463**(7282), 763–768.
- International Wheat Genome Sequencing Consortium (IWGSC) (2014) A chromosome-based draft sequence of the hexaploid bread wheat (*Triticum aestivum*) genome. *Science*, **345**(6194), 125178.

- Kandul, N.P. and Noor, M.A. (2009) Large introns in relation to alternative splicing and gene evolution: a case study of *Drosophila* bruno-3. *BMC Genet.* **10**, 67.
- Kim, E., Magen, A. and Ast, G. (2006) Different levels of alternative splicing among eukaryotes. *Nucleic Acids Res.* **35**(1), 125–131.
- Kornblihtt, A.R., Schor, I.E., Alló, M., Dujardin, G., Petrillo, E. and Muñoz, M.J. (2013) Alternative splicing: a pivotal step between eukaryotic transcription and translation. *Nat. Rev. Mol. Cell Biol.* **14**(3), 153–165.
- Li, C. and Dubcovsky, J. (2008) Wheat FT protein regulates VRN1 transcription through interactions with FDL2. *Plant J.* **55**(4), 543–554.
- Li, C., Lin, H. and Dubcovsky, J. (2015) Factorial combinations of protein interactions generate a multiplicity of florigen activation complexes in wheat and barley. *Plant J.* **84**(1), 70–82.
- López-González, L., Mouriz, A., Narro-Diego, L., Bustos, R., Martínez-Zapater, J.M., Jarillo, J.A. and Piñeiro, M. (2014) Chromatin-dependent repression of the Arabidopsis floral integrator genes involves plant specific PHD-containing proteins. *Plant Cell*, **26**(10), 3922–3938.
- Lu, F.L., Cui, X., Zhang, S.B., Liu, C.Y. and Cao, X.F. (2010a) JM14 is an H3K4 demethylase regulating flowering time in Arabidopsis. *Cell Res.* **20**(3), 387–390.
- Lu, T., Lu, G., Fan, D. et al. (2010b) Function annotation of the rice transcriptome at single-nucleotide resolution by RNA-seq. *Genome Res.* **20**(9), 1238–1249.
- Lucio, R.F., Pan, Q., Tominaga, K., Blencowe, B.J., Pereira-Smith, O.M. and Misteli, T. (2010) Regulation of alternative splicing by histone modifications. *Science (New York, N.Y.)*, **327**(5968), 996–1000.
- Lv, B., Nitcher, R., Han, X., Wang, S., Ni, F., Li, K., Pearce, S., Wu, J., Dubcovsky, J. and Fu, D. (2014) Characterization of FLOWERING LOCUS T1 (FT1) gene in *Brachypodium* and wheat. *PLoS ONE*, **9**(4), e94171.
- McGuire, A.M. (2008) Cross-kingdom patterns of alternative splicing and splice recognition. *Genome Biol.* **9**(3), R50.
- Mercer, T.R., Edwards, S.L., Clark, M.B., Neph, S.J., Wang, H., Stergachis, A.B., Stamatoyannopoulos, J.A. (2013) DNase I-hypersensitive exons colocalize with promoters and distal regulatory elements. *Nat. Genet.* **45**(8), 852–859.
- Molitor, A.M., Bu, Z., Yu, Y. and Shen, W.H. (2014) Arabidopsis AL PHD-PRC1 complexes promote seed germination through H3K4me3-to-H3K27me3 chromatin state switch in repression of seed developmental genes. *PLoS Genet.* **10**(1), 229–231.
- Navarro, C., Cruz-Oro, E. and Prat, S. (2015) Conserved function of FLOWERING LOCUS T (FT) homologues as signals for storage organ differentiation. *Curr. Opin. Plant Biol.* **23**, 45–53.
- Ong-Abdullah, M., Ordway, J.M., Jiang, N. et al. (2015) Loss of Karma transposon methylation underlies the mantled somaclonal variant of oil palm. *Nature*, **525**(7570), 533–537.
- Pandya-Jones, A. and Black, D.L. (2009) Co-transcriptional splicing of constitutive and alternative exons. *RNA*, **15**(10), 1896–1908.
- de la Paz Sanchez M. and Gutierrez, C. (2009) Arabidopsis ORC1 is a PHD-containing H3K4me3 effector that regulates transcription. *Proc. Natl Acad. Sci. USA*, **106**(6), 2065–2070.
- Pin, P.A. and Nilsson, O. (2012) The multifaceted roles of FLOWERING LOCUS T in plant development. *Plant Cell Environ.* **35**(10), 1742–1755.
- Qian, S., Lv, X., Scheid, R.N. et al. (2018) Dual recognition of H3K4me3 and H3K27me3 by a plant histone reader SHL. *Nat. Commun.* **9**(1), 2425.
- Qin, Z., Wu, J., Geng, S. et al. (2017) Regulation of FT splicing by an endogenous cue in temperate grasses. *Nat. Commun.* **8**, 14320.
- Ream, T.S., Woods, D.P., Schwartz, C.J., Sanabria, C.P., Mahoy, J.A., Walters, E.M., Kaeppler, H.F. and Amasino, R.M. (2014) Interaction of photoperiod and vernalization determines flowering time of *Brachypodium distachyon*. *Plant Physiol.* **164**(2), 694–709.
- Rincon-Arango, H., Halow, J., Delrow, J.J., Parkhurst, S.M. and Groudine, M. (2012) UpSET recruits HDAC complexes and restricts chromatin accessibility and acetylation at promoter regions. *Cell*, **151**(6), 1214–1228.
- Roy, M., Kim, N., Xing, Y. and Lee, C. (2008) The effect of intron length on exon creation ratios during the evolution of mammalian genomes. *RNA (New York, N.Y.)*, **14**(11), 2261–2273.
- Schwartz, C.J., Doyle, M., Manzaneda, A.J., Rey, P.J., Mitchell-Olds, T. and Amasino, R.M. (2010) Natural variation of flowering time and vernalization responsiveness in *Brachypodium distachyon*. *Bioenergy Res.* **3**(1), 38–46.
- Shan, Q., Wang, Y., Chen, K. et al. (2013) Rapid and efficient gene modification in rice and *Brachypodium* using TALENs. *Mol. Plant*, **6**(4), 1365–1368.
- Shi, X., Hong, T., Walter, K.L. et al. (2006) ING2 PHD domain links histone H3 lysine 4 methylation to active gene repression. *Nature*, **442**(7098), 96–99.
- Shukla, S. and Oberdoerffer, S. (2012) Co-transcriptional regulation of alternative pre-mRNA splicing. *Biochem. Biophys. Acta*, **1819**(7), 673–683.
- Song, S., Qi, T., Huang, H. et al. (2011) The Jasmonate-ZIM domain proteins interact with the R2R3-MYB transcription factors MYB21 and MYB24 to affect Jasmonate-regulated stamen development in Arabidopsis. *Plant Cell*, **23**(3), 1000–1013.
- Song, Y.H., Shim, J.S., Kinmonth-Schultz, H.A. and Imaizumi, T. (2015) Photoperiodic flowering: time measurement mechanisms in leaves. *Annu. Rev. Plant Biol.* **66**, 441–464.
- Spies, N., Nielsen, C.B., Padgett, R.A. and Burge, C.B. (2009) Biased chromatin signatures around polyadenylation sites and exons. *Mol. Cell*, **36**(2), 245–254.
- Srikanth, A. and Schmid, M. (2011) Regulation of flowering time: all roads lead to Rome. *Cell Mol. Life Sci.* **68**(12), 2013–2037.
- Sun, J., Qi, L., Li, Y., Zhai, Q. and Li, C. (2013) PIF4 and PIF5 transcription factors link blue light and auxin to regulate the phototropic response in Arabidopsis. *Plant Cell*, **25**(6), 2102–2114.
- Tamada, Y., Yun, J.Y., Woo, S.C. and Amasino, R.M. (2009) ARABIDOPSIS TRITHORAX-RELATED7 is required for methylation of lysine 4 of histone H3 and for transcriptional activation of FLOWERING LOCUS C. *Plant Cell*, **21**(10), 3257–3269.
- Tamaki, S., Matsuo, S., Wong, H.L., Yokoi, S. and Shimamoto, K. (2007) Hd3a protein is a mobile flowering signal in rice. *Science*, **316**(5827), 1033–1036.
- Taoka, K., Ohki, I., Tsuji, H., Kojima, C. and Shimamoto, K. (2013) Structure and function of florigen and the receptor complex. *Trends Plant Sci.* **18**(5), 287–294.
- Tian, Y., Jia, Z., Wang, J. et al. (2011) Global mapping of H3K4me1 and H3K4me3 reveals the chromatin state-based cell type-specific gene regulation in human Treg cells. *PLoS ONE*, **6**(11), e27770.
- Waadt, R., Schmidt, L.K., Lohse, M., Hashimoto, K., Bock, R. and Kudla, J. (2008) Multicolor bimolecular fluorescence complementation reveals simultaneous formation of alternative CBL/CIPK complexes in planta. *Plant J.* **56**(3), 505–516.
- Wigge, P.A. (2011) FT, a mobile developmental signal in plants. *Curr. Biol.* **21**(9), R374–378.
- Woods, D.P., Ream, T.S., Minevich, G., Hobert, O. and Amasino, R.M. (2014) PHYTOCHROME C is an essential light receptor for photoperiodic flowering in the temperate grass, *Brachypodium distachyon*. *Genetics*, **198**, 397–408.
- Wu, L., Liu, D., Wu, J., Zhang, R., Qin, Z., Liu, D., Li, A., Fu, D., Zhai, W. and Mao, L. (2013) Regulation of FLOWERING LOCUS T by a microRNA in *Brachypodium distachyon*. *Plant Cell*, **25**(11), 4363–4377.
- Wysocka, J., Swigut, T., Xiao, H. et al. (2006) A PHD finger of NURF couples histone H3 lysine 4 trimethylation with chromatin remodelling. *Nature*, **442**(7098), 86–90.
- Yang, H., Mo, H., Fan, D., Cao, Y., Cui, S. and Ma, L. (2012) Overexpression of a histone H3K4 demethylase, JM15, accelerates flowering time in Arabidopsis. *Plant Cell Report*, **31**(7), 1297–1308.
- Yu, C.W., Liu, X., Luo, M., Chen, C., Lin, X., Tian, G., Lu, Q., Cui, Y. and Wu, K. (2011) HISTONE DEACETYLASE6 interacts with FLOWERING LOCUS D and regulates flowering in Arabidopsis. *Plant Physiol.* **156**(1), 173–184.
- Zhang, Y., Zhang, F., Li, X., Baller, J.A., Qi, Y., Starker, C.G., Bogdanov, A.J. and Voytas, D.F. (2013) TALENs enable efficient plant genome engineering. *Plant Physiol.* **161**(1), 20–27.